BNL-212024-2019-JAAM

Potassium-Promoted Reduction of Cu2O/Cu(111) by CO

J. A. Rodriguez,

To be published in "Journal of Physical Chemistry C"

April 2019

Chemistry Department

Brookhaven National Laboratory

U.S. Department of Energy

USDOE Office of Science (SC), Basic Energy Sciences (BES) (SC-22)

Notice: This manuscript has been authored by employees of Brookhaven Science Associates, LLC under Contract No. DE-SC0012704 with the U.S. Department of Energy. The publisher by accepting the manuscript for publication acknowledges that the United States Government retains a non-exclusive, paid-up, irrevocable, world-wide license to publish or reproduce the published form of this manuscript, or allow others to do so, for United States Government purposes.

DISCLAIMER

This report was prepared as an account of work sponsored by an agency of the United States Government. Neither the United States Government nor any agency thereof, nor any of their employees, nor any of their contractors, subcontractors, or their employees, makes any warranty, express or implied, or assumes any legal liability or responsibility for the accuracy, completeness, or any third party's use or the results of such use of any information, apparatus, product, or process disclosed, or represents that its use would not infringe privately owned rights. Reference herein to any specific commercial product, process, or service by trade name, trademark, manufacturer, or otherwise, does not necessarily constitute or imply its endorsement, recommendation, or favoring by the United States Government or any agency thereof or its contractors or subcontractors. The views and opinions of authors expressed herein do not necessarily state or reflect those of the United States Government or any agency thereof.

Potassium-Promoted Reduction of $Cu_2O/Cu(111)$ by CO

Iradwikanari Waluyo,[†,§] Kumudu Mudiyanselage,[†,∥] Fang Xu,[†,⊥] Wei An,[†,#] Ping Liu,[†] J. Anibal Boscoboinik,[‡] José A. Rodriguez,[†] and Dario J. Stacchiola*[,†]

[†]Chemistry Department, Brookhaven National Laboratory, Upton, New York 11973, United States

[‡]Center for Functional Nanomaterials, Brookhaven National Laboratory, Upton, New York 11973, United States

ABSTRACT: In situ X-ray photoelectron spectroscopy (XPS), infrared reflection absorption spectroscopy (IRRAS), and scanning tunneling microscopy (STM) were used to study the reduction of potassium-modified $Cu_2O/Cu(111)$ by CO. By following the time evolution of the O 1s peak of Cu_2O, we determined that the apparent activation energy for Cu_2O reduction by 2×10^{-4} Torr CO is decreased by ~30% in the presence of K. On the K-modified surface, both XPS and IRRAS data show the formation of a surface species identified by IRRAS as carbonate (CO_3^{2-}), likely forming a K^+-CO_3^{2-} complex, which is stable up to 500 K. STM images show that K^+-CO_3^{2-} complexes form chains around reduced Cu islands, thereby hindering the mass transfer of Cu atoms and preventing the reconstruction of the surface. Theoretical calculations show that the formation of carbonate on the K-modified "44" Cu_2O structure is thermodynamically favorable compared to the formation of CO_2 on either the bare or K-modified surfaces.

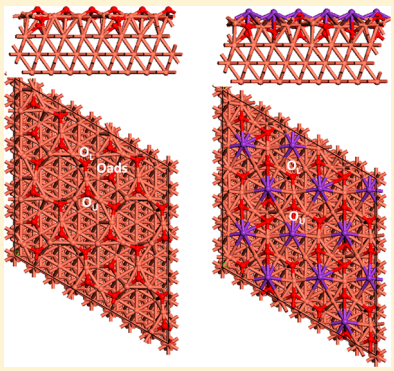

■ INTRODUCTION

The addition of alkali promoters has long been known to enhance the activity of supported transition metal catalysts for a variety of industrially important reactions such as ammonia synthesis,[1] CO_2 hydrogenation,[2] benzyl alcohol oxidation,[3] ethylene epoxidation,[4] and preferential CO oxidation in the presence of H_2 (PROX).[5−7] On single crystal metal surfaces, the coadsorption of alkali metals and surface species such as CO, CO_2, H_2O, and O has been extensively studied.[8,9] The coadsorption of alkali metals and CO, for example, results in the increased heat of adsorption of both CO and the alkali metal[10,11] as well as a red-shift of the CO IR stretch frequency.[12−14] Various models have been proposed to explain the alkali-promoted CO stabilization on metal surfaces, generally involving the weakening of the internal C−O bond and strengthening of the metal−CO bond.[9,15−22] In addition, although CO_2 tends to adsorb weakly on transition metal surfaces, the highly electropositive alkali metals have been found to activate CO_2 through electron donation, resulting in the formation of various negatively charged species, including carbonate (CO_3^{2-}), oxalate ($C_2O_4^{2-}$), carboxylate (CO_2^{-}), and carbonite (CO_2^{2-}), with carbonate being considered as the most stable.[23−26] An infrared reflection absorption spectroscopy (IRRAS) study recently showed that at low temperatures, potassium multilayers promote the formation of formate from CO_2 and H_2O through the activation of CO_2 and the dissociation of H_2O.[27]

Alkalis are widely used in the industry for promoting catalysts.[28,29] Despite extensive research, proposed mechanisms of alkali promotion for various catalytic reactions remain controversial. This is partly due to the lack of in situ characterization studies on the promoting effect during reaction conditions. In ammonia synthesis, potassium atoms are considered to be localized at the active centers present on the surface to enhance the activity.[30] In Fischer−Tropsch synthesis, the strong basicity of potassium promotes the adsorption of reactants (CO and H_2) on the active sites, which effects activity and selectivity.[31]

The effect of alkali promoters on metal oxide films has not been studied in situ as extensively using surface science techniques due to the high complexity of these systems, as reported previously for ammonia synthesis.[32] Since the identification of the role of promoters is essential for the enhancement of the activity, it is very important to carry in situ investigations of the role of promoters in model systems using surfaces science techniques, which provides molecular level mechanistic information.

Cu can be easily oxidized to Cu_2O under ultrahigh vacuum (UHV) conditions and can be further oxidized to CuO at higher temperatures and O_2 pressures.[33] The interaction between CO and copper surfaces has been extensively studied because Cu-based catalysts are a well-known class of heterogeneous catalysts in CO conversion reactions such as CO oxidation ($2CO + O_2 \rightarrow 2CO_2$),[34,35] methanol synthesis ($CO + 2H_2 \rightarrow CH_3OH$),[36,37] and the water−gas shift reaction ($CO + H_2O \rightarrow CO_2 + H_2$).[38] In the case of copper oxide (Cu_xO_y) catalysts, their activity for CO oxidation depends on the oxidation state of Cu, with a decreasing activity and increasing activation energy observed with increasing oxidation state of Cu.[39,40]

Special Issue: Hans-Joachim Freund and Joachim Sauer Festschrift

Received: July 31, 2018
Revised: October 8, 2018
Published: November 8, 2018

CO is known to be able to reduce Cu_2O to metallic Cu via the Mars-van Krevelen mechanism in which CO reacts with an oxygen atom from the oxide surface and forms CO_2. The kinetics of this reaction can also be considered as a model for the initial rate of the CO + O step in the CO oxidation reaction in a highly reducing environment, thereby avoiding the decreased catalytic activity due to the oxidation of Cu^+ to Cu^{2+} by O_2. The reduction of Cu_2O/Cu(111) by CO was studied using scanning tunneling microscopy (STM) and X-ray photoelectron spectroscopy (XPS) under UHV conditions.[41] A two-stage process was observed: a slow initial stage or induction process in which CO reacts with chemisorbed oxygen atoms, creating an O-deficient Cu_2O phase, followed by a fast stage in which CO reacts with the lattice oxygen atoms of Cu_2O.[41] Ambient pressure STM experiments revealed that Cu_2O reduction starts at defect sites, and the mass transfer of released Cu from terraces to step-edges causes the formation of metallic phase fronts that propagate across the surface, resulting in the reconstruction of the step-edges and separation of the oxide and metallic phases.[42]

In this work, in situ XPS, IRRAS, and STM were used to study the effect of K on the reduction of Cu_2O/Cu(111) by CO. We show that K promotes the reduction of Cu_2O by CO and reduces the activation energy of the reaction by ~30%. The reduction of K/Cu_2O/Cu(111) by CO results in the formation of a surface species that can be identified as carbonate (CO_3^{2-}), which forms chains and islands around the reduced Cu islands. This is supported by results from theoretical calculations, which show that K stabilizes the formation of CO_3^{2-} on the surface. Since CO needs to react with two O surface atoms in order to form CO_3^{2-}, the favorable formation of CO_3^{2-} due to the presence of K, therefore, accelerates the reduction of the surface.

■ EXPERIMENTAL METHODS

XPS measurements were performed at beamline X1A1 at the National Synchrotron Light Source (NSLS). The endstation was equipped with a differentially pumped hemispherical electron analyzer (SPECS Phoibos 150 NAP). A 300 μm entrance aperture to the first differential pumping stage was located >0.5 mm from the sample. The sample was heated using a ceramic button heater, and the sample temperature was measured by a K-type thermocouple spot-welded to a Ta foil placed between the sample and the heater. XP spectra were obtained with a pass energy of 10 eV and photon energies of 689 and 523 eV for the O 1s and C 1s regions, respectively.

IRRAS experiments were performed in a combined UHV surface analysis chamber and elevated-pressure reactor/IRRAS cell system. The elevated-pressure cell was coupled to a Bruker IFS 66v/s Fourier-transform infrared (FT-IR) spectrometer. The Cu(111) single crystal was held tightly using a Ta loop embedded in a groove machined around the crystal edge. The Ta loop was attached directly to the manipulator feed-through, which was used for both mechanical support and heating/cooling. The sample temperature was measured by a K-type thermocouple attached to the top edge of the crystal. IRRA spectra were collected at 4 cm^{-1} resolution using a grazing angle of approximately 85° to the surface normal.[43]

STM experiments were performed using a SPECS Aarhus HT-NAP STM, which contained a sealed ambient pressure cell housed in a UHV chamber. A commercial etched tungsten tip was used for all of the scanning under constant current mode. Images were scanned from bottom to top, and each image took ~150 s to obtain.

In all experiments, Cu(111) was cleaned by repeated cycles of Ar^+ sputtering and 800−850 K annealing. The sample was then annealed to 550−650 K in 5×10^{-7} Torr O_2 for 20 min, resulting in the formation of well-ordered Cu_2O(111)-"44" film.[44] K was evaporated using a K getter source from SAES. The coverage of K was calibrated using a quartz crystal microbalance (QCM) for XPS experiments and by Auger electron spectroscopy for IRRAS experiments. The CO stretch IR peak was also used to confirm the amount of K on the surface as its frequency was sensitive to K coverage. Since the deposition of K caused a partial reduction of Cu_2O, the as-deposited surface was then reoxidized at 500 K under 5×10^{-7} Torr O_2 for 10 min. For the reduction experiments, CO was introduced to the chamber via a variable leak valve. CO pressures were read by a hot cathode/MicroPirani combination gauge (XPS), a Pirani gauge (IRRAS), and a baratron gauge (STM).

■ THEORETICAL METHODS

Calculations were performed by using periodic density functional theory (DFT) as implemented in the Vienna ab initio simulation package (VASP).[45,46] Ion-core electron interactions were described using the projected augmented wave method (PAW),[47,48] and Perdew−Wang functional (GGA-PW91) within the generalized gradient approximation (GGA)[49,50] was used to describe exchange-correlation effects. The cutoff energy of the plane-wave basis set was 400 eV. To model the "44" structure, we built a Cu_2O-like O−Cu−O overlayer on top of a three-layer $p(4 \times 4)$ Cu(111) slab. Nine Cu ions and seven O ions were included in the oxide layer.[51] Figure 1(a) shows the optimized "44" structure where O_U and O_L represent lattice oxygen atoms in the upper and lower layers, respectively, and O_{ads} is a chemisorbed oxygen atom. Here, $x = 1.3$ according to the ratio between Cu and O on the

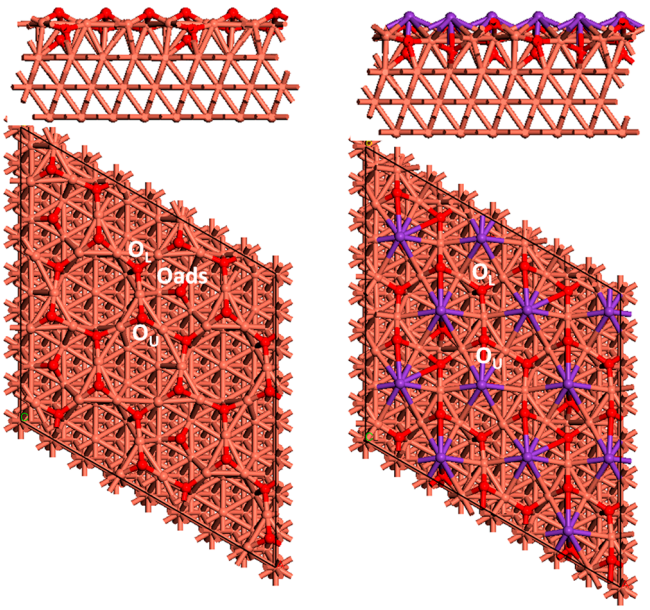

Figure 1. Optimized structures for (a) the "44" structure and (b) 0.19 ML K deposited on the "44" structure. Three types of O atoms on the surface are labeled. O_{ads}: chemisorbed O; O_U: upper layer O; O_L: lower layer O. Red: O, reddish brown: Cu, purple: K.

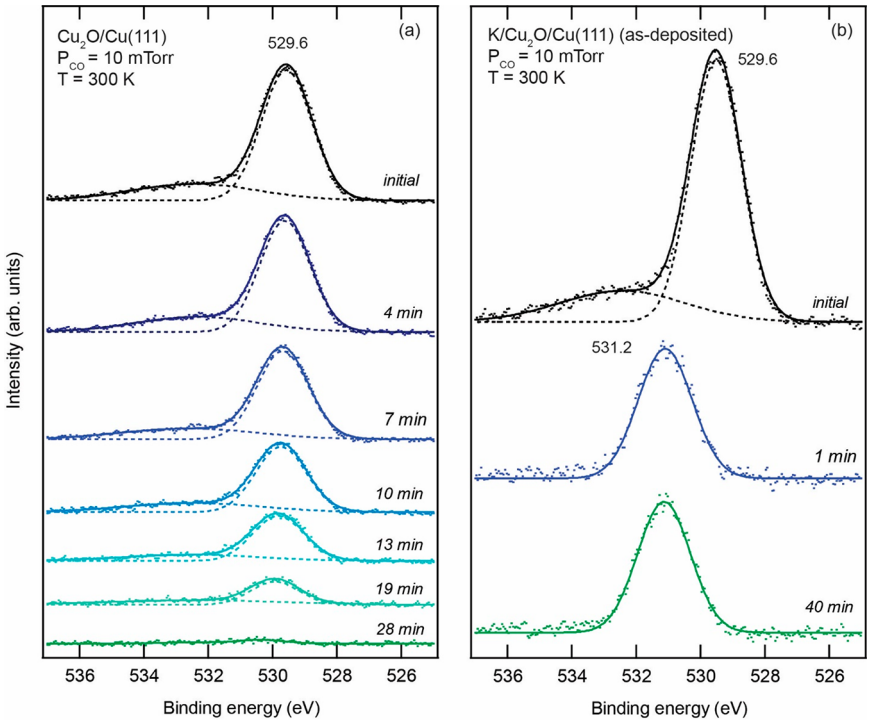

Figure 2. Time-dependent O 1s AP-XP spectra during the reduction of (a) $Cu_2O/Cu(111)$ and (b) as-deposited $K/Cu_2O/Cu(111)$ by 10 mTorr of CO at 300 K.

O−Cu−O layer. To model the K-deposited "44" structure (Figure 1(b)), we added additional O to the center of the O−Cu−O hexagonal ring and K on top of each chemisorbed O atoms.[52] Such an arrangement corresponds to our experimental procedures and calculated K binding orderings, i.e., −2.44 eV ← 2.75 eV ← 3.23 eV for O_U, O_L, and O_{ads}, respectively, in which K binds O_{ads} the strongest. As such, a 0.19 ML K is formed on the "44" structure. A vacuum of 20 Å between the slabs was applied perpendicular to the surface. The conjugate gradient algorithm was used in optimization, allowing a convergence of 10^{-4} eV in total energy and 0.02 eV/Å in Hellmann−Feynman force on each atom. The Brillouin-zone integration was sampled by 3 × 3 × 1 k-points using the Monkhorst−Pack scheme.[53] All atoms were allowed to relax except those of the bottom two layers that were fixed at the bulk position with the optimized lattice constant of 3.634 Å.

The binding energy (BE) was defined as $BE = E_{ads/slab} - E_{slab} - E_{ads(gas)}$, where ads is CO, CO_2, or K, slab is the bare "44" or K-deposited "44" structure, and $E_{ads/slab}$, E_{slab}, and $E_{ads(gas)}$ are the total energy of adsorbate/slab, clean slab, and a free adsorbate in gas phase, respectively. Negative (positive) BE represents exothermic (endothermic) adsorption process. The reaction energy of CO titration for high pressure of CO was calculated as $\Delta E = E_{mOv} + mE_{CO2(g)} - mE_{CO(g)} - E_0$ based on $CO_{(g)} + O_{bulk} \rightarrow O_V + CO_{2(g)}$, where m represents the total number of O_V. E_{Ov}, $E_{CO2(g)}$, $E_{CO(g)}$, and E_0 represent the total energy of a slab with oxygen vacancies (O_V), gas-phase CO_2, gas-phase CO, and a slab without Ov, respectively. By including the $T\Delta S$ term, we also calculated the Gibbs reaction energy (ΔG_{rxn}).

■ EXPERIMENTAL RESULTS

Figure 2 displays the XP spectra of the O 1s region when $Cu_2O/Cu(111)$ and $K/Cu_2O/Cu(111)$ were exposed to 10 mTorr of CO at 300 K. The initial main peak at 529.6 eV is assigned to the lattice oxygen of Cu_2O, while the higher energy tail at 532.3 eV can be attributed either to surface OH from the adsorption of background H_2O or to strongly chemisorbed oxygen.[54] In the absence of K (Figure 2(a)), the oxide peak intensity decreases over time as the O atoms from Cu_2O is consumed by CO and Cu^+ is reduced to Cu^0. At the CO pressure used in the current study, only a negligible (i.e., 1−2 min) induction period was observed, as opposed to low pressure previous studies.[41] The reaction is complete after 28 min as evidenced by the disappearance of the O 1s peak. In the C 1s region, only a small C^0 peak is observed after the reaction (not shown). The reaction rate for the reduction of a Cu_2O film at 300 K is determined to be $(1.6 \pm 0.1) \times 10^{-3}$ s^{-1}, in good agreement with a similar AP-XPS measurement in a previous study[42] yielding a reaction rate of $(2.1 \pm 0.1) \times 10^{-3}$ s^{-1} at the same temperature and CO pressure. By performing similar experiments at 325 and 350 K, we determined an apparent activation energy of 0.16 ± 0.02 eV for the reduction of $K/Cu_2O/Cu(111)$ by 10 mTorr CO, which is lower than the previously reported 0.22 ± 0.01 eV for the reduction of $Cu_2O/Cu(111)$ by 1 mTorr of CO.[55]

With ∼0.1 monolayers of K deposited on the surface, the same initial main oxide peak at 529.6 eV is observed before the onset of reduction by 10 mTorr CO (Figure 2(b)), indicating no incorporation of new surface species due to the potential contamination from the deposition of K; but instead of a gradual intensity decrease, a new peak appears at 531.2 eV after only 1 min of CO exposure, and it is unchanged with longer CO exposure. This indicates that Cu_2O reduction is already complete after 1 min and a different O-containing surface species is formed and that K promotes the reduction of Cu_2O by CO. The fast reduction of the K-modified Cu_2O film under the above conditions does not allow for obtaining kinetic data. In order to determine the reaction rate and activation energy, a lower pressure of CO (2×10^{-4} Torr) was used to reduce

reoxidized $K/Cu_2O/Cu(111)$, in order to start with a fully oxidized film as for the case of the reduction of pure Cu_2O films. Figure 3 shows the time-dependent O 1s spectra during

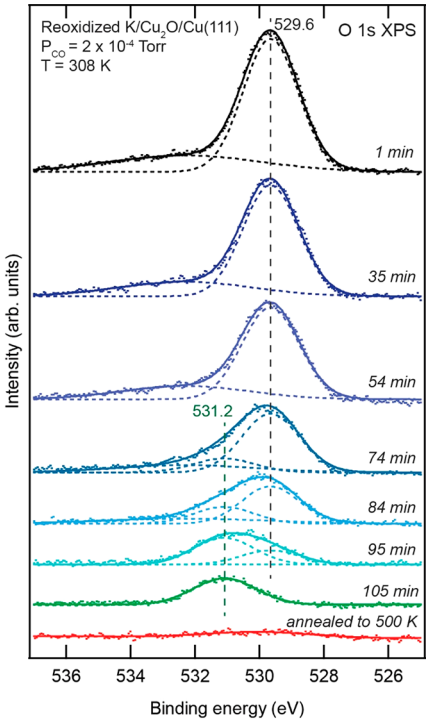

Figure 3. Time-dependent O 1s XP spectra during the reduction of reoxidized $K/Cu_2O/Cu(111)$ by 2×10^{-4} Torr CO at 308 K, followed by annealing of the reduced surface to 500 K.

this reaction at 308 K; similar experiments were performed at 323 and 348 K. While the expected intensity decrease of the oxide peak at 529.6 eV is observed as Cu_2O is reduced, a new component at 531.2 eV starts to appear after ~74 min and increases thereafter, until it becomes the only peak at 105 min. This peak disappears after the sample was annealed to 500 K. An apparent activation energy of 0.28 ± 0.01 eV was determined for the reduction of reoxidized $K/Cu_2O/Cu(111)$ by 2×10^{-4} Torr of CO. The same lower CO pressure was used to reduce $Cu_2O/Cu(111)$ at higher temperatures (473, 488, and 503 K), and an apparent activation energy of 0.42 ± 0.01 eV was obtained. This represents an ~30% decrease in activation energy due to the presence of K at the same CO pressure. The difference in the apparent activation energies for $Cu_2O/Cu(111)$ reduction at different CO pressures (i.e., 0.42 eV at 0.1 mTorr CO, 0.22 eV at 1 mTorr CO, and 0.15 eV at 10 mTorr CO) is due to the different amounts of CO available on the surface.

Figure 4 shows the K 2p and C 1s XP spectra obtained before and after the reduction by 2×10^{-4} Torr CO as well as after a 500 K annealing of the sample. Before reduction, the K $2p_{3/2}$ peak has a binding energy of 293.2 eV. A K $2p_{3/2}$ binding energy range between 292.89 and 293.49 eV was reported for K_2O-SiO_2 glasses depending on the mole fraction of K_2O.[56] This indicates that for the reoxidized $K/Cu_2O/Cu(111)$ sample, K is likely oxidized as K_2O. However, the O 1s signal from K_2O is indistinguishable from that from Cu_2O as no additional features or binding energy shifts are observed in the O 1s spectra obtained after K evaporation and reoxidation. In fact, the O 1s spectra of $Cu_2O/Cu(111)$, as-deposited $K/Cu_2O/Cu(111)$, and reoxidized $K/Cu_2O/Cu(111)$ look nearly identical except for small differences in overall intensity. After reduction, two peaks are observed in the C 1s region at 288.9 and 284.2 eV. The 288.9 eV peak can be assigned to a C_xO_y surface species that also gives rise to the 531.2 eV peak in the O 1s region, while the 284.2 eV is attributed to C^0. The K 2p peaks only show a small shift by 0.3 eV to higher binding energy, suggesting that K remains in the +1 oxidation state, forming a complex with the anionic C_xO_y species. The 288.9 eV peak disappears upon annealing to 500 K, consistent with the O 1s spectra. The fact that the C^0 peak does not increase in intensity with the disappearance of the 288.9 eV peak indicates that complete desorption instead of decomposition of the C_xO_y species occurs upon annealing to 500 K. After the 500 K anneal, K^+ is reduced to K^0 as evidenced by the shift of the K $2p_{3/2}$ peak to 294.3 eV, in agreement with the K $2p_{3/2}$ binding energy of 294.2 eV for K/Cu(111) (not shown). The shift of the K 2p spectrum to higher binding energy due to the reduction of K^+ to metallic K has been well documented in the literature.[57] In addition, the apparent broadening of the K $2p_{1/2}$ peak and the fact that the two spin orbit peaks of K 2p no longer display the expected 1:2 intensity ratio is likely due to the presence of plasmon loss features, which are typical for metallic K.[57,58] Although plasmon features are normally observed for high coverages of K, they can also be caused by the formation of metallic K clusters.[57] This further supports the reduction of K^+ to K^0 that accompanies the desorption of the C_xO_y species when the sample was heated to 500 K. The lower overall intensity of the K 2p spectra after heating to 500 K is likely because some K has desorbed at this temperature.

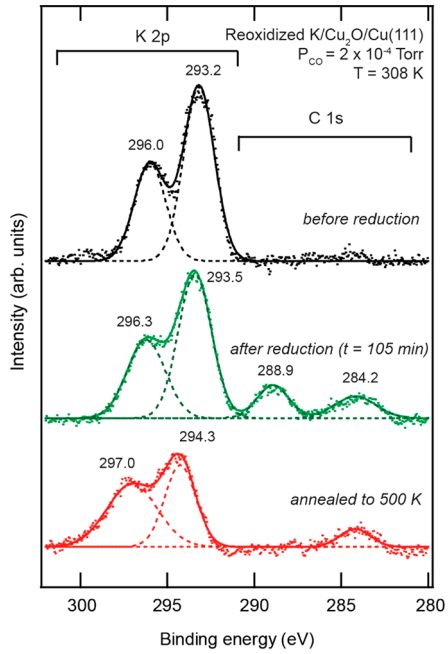

Figure 4. K 2p and C 1s XP spectra of reoxidized $K/Cu_2O/Cu(111)$ before (top) and after (middle) reduction by 2×10^{-4} Torr CO at 308 K as well as after annealing the reduced surface to 500 K (bottom). The spectra were taken in the same experiment as Figure 2.

While XPS unambiguously shows the formation of a C_xO_y species, vibrational spectroscopy can help in identifying the adsorbed species. Figure 5(a) shows the time-dependent IRRA spectra obtained when reoxidized $K/Cu_2O/Cu(111)$ was continuously exposed to 2×10^{-4} Torr CO at 300 K. Before

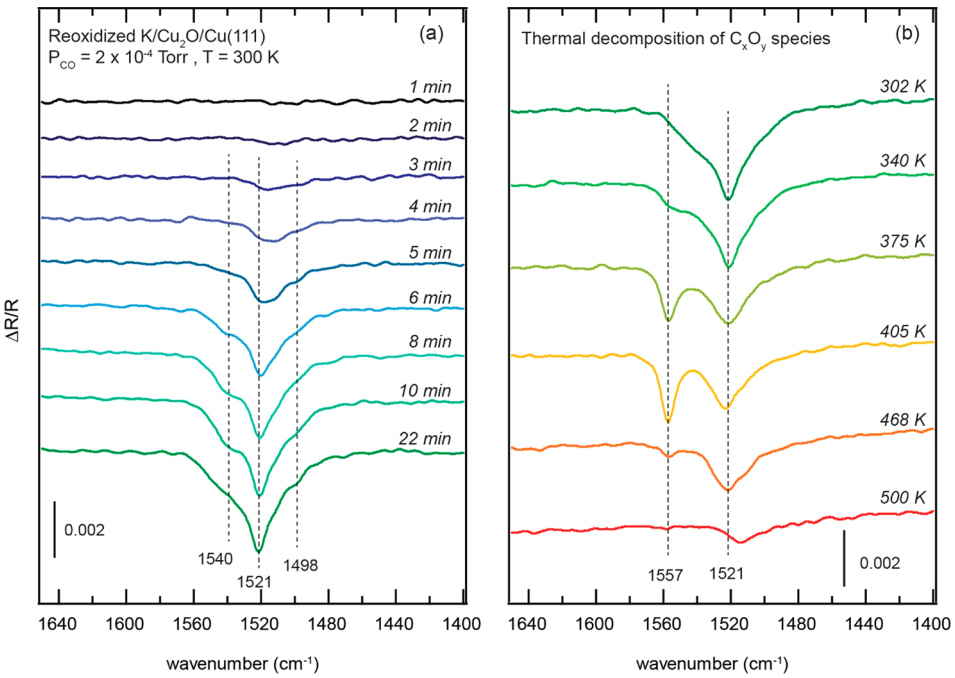

Figure 5. (a) Time-dependent IRRA spectra of reoxidized $K/Cu_2O/Cu(111)$ exposed to CO at a constant pressure of 2×10^{-4} Torr at 300 K. (b) IRRA spectra measured after heating the reduced sample to the specified temperatures.

the onset of reduction, no peaks were observed in the 1000–2800 cm^{-1} region. As the reduction reaction proceeds, a surface species is formed as evidenced by the appearance of a peak in the OCO stretch region at ~1500 cm^{-1}, which grows in intensity as a function of reaction time. Upon completion of the reduction reaction, the peak has a maximum intensity at 1521 cm^{-1} with shoulders at 1498 and 1540 cm^{-1}. No other peaks were observed between 1000 and 2800 cm^{-1}. Figure 5(b) shows that the C_xO_y species starts to decompose above 340 K when the intensity of the 1521 cm^{-1} peak starts to decrease. At the same time, a new peak is observed at 1557 cm^{-1}. This higher frequency peak disappears first at 468 K, while the intensity of the 1521 cm^{-1} peak is unchanged. Both peaks almost disappear at 500 K, indicating the desorption of the species and in agreement with the XP spectra.

Since the reduction of Cu_2O involves the formation of CO_2, the identification of the C_xO_y species benefits from the comparison with the vibrational frequencies of various species formed from the adsorption of CO_2 and CO on related systems, as summarized in Table 1. A definitive assignment is nontrivial because all of these species ($C_2O_4^{2-}$, CO_3^{2-}, CO_2^{-}, and CO_2^{2-}) have overlapping OCO stretch modes between 1000 and 1900 cm^{-1}. In light of the observation of ordered structures of this species by STM, oxalate ($C_2O_4^{2-}$) seems to be a likely candidate since the self-assembly of oxalic acid on Cu(111) has been observed at room temperature.[59] However, oxalate (both C_{2v} and D_{2h} symmetries) can be ruled out spectroscopically because it has prominent ν_a(OCO) and ν_s(OCO) modes at around 1600–1700 cm^{-1} and ~1300–1400 cm^{-1}, respectively, and no peaks at ~1500 cm^{-1} (Table 1). CO_2^{-} stretch modes generally have frequencies close to those of oxalate, while CO_2^{2-} only has modes below 1400 cm^{-1}. A 1530 cm^{-1} peak observed from the coadsorption of Na and CO_2 on Pd(111) was assigned to the ν_a(OCO) of a CO_2^{-} species; however, there is also a stronger accompanying

Table 1. Frequencies of the CO Stretching Modes of Various C_xO_y Species on Relevant Surfaces

	ν_a(CO)	ν_s(CO)	ref
Oxalates ($C_2O_4^{2-}$)			
K + CO_2/Cu(111) (D_{2h})	1642	1320	24
K + CO_2/Cu(111) (C_{2v})	1718	1574	24
CO_2 on $\sqrt{3}\times\sqrt{3}$-R30°-K/Ru(001)	1600–1725	1342	23
CO_2 on multilayer-K/Ru(001)	1625	1345	23
K + CO_2/Co(1010)	1625	1312	71
CO_2 + H_2O + K on Cu(111) annealed to 475 K	1665	1315	27
Carbonates (CO_3^{2-})			
CO_2 on $\sqrt{3}\times\sqrt{3}$-R30°-K/Ru(001)	1467		23
CO_2 on multilayer-K/Ru(001)	1447	1071 (vw)	23
CO_2 + H_2O + K on Cu(111) annealed to 600 K	1460		27
K + CO_2/Cu(110) annealed > 233 K	1512	1045 (w)	72
CO on Cs/Cu(110)-O	1510	1050 (w)	61
CO + O_2 on Cs/Cu(110)	1500	1050 (w)	61
CO_2 on Cs/Cu(110)	1510	1060 (w)	61
CO on K/Cu2O/Cu(111)	1521		*this work*
Carboxylate (CO_2^{-})			
K + CO_2/Pt(111)	1600	1340	26
Na + CO_2/Pd(111)	1530	1210	25
K + CO_2/Au(111)	1620	1350	73
Carbonite (CO_2^{2-})			
CO_2 on multilayer-K/Ru(001)	1396	1133	23
CO/CeO_2 (C_{2v})	1317	1150	74
CO/CeO_2 (C_s)	1266	1071	74

peak at 1210 cm^{-1} assigned to ν_s(OCO), which we do not observe in our experimental data.

Carbonates have a strong ν(OCO) mode between 1350 and 1700 cm^{-1} depending on the sample and bonding configuration, while other modes are either very weak or not observed.[60] A strong carbonate peak at ~1460 cm^{-1} was observed after annealing coadsorbed CO_2 and K on Ru(001) to 420 K, and it remains stable up to 650 K.[24] Similarly, the reaction between CO_2 and H_2O on K multilayers on Cu(111) produces a strong carbonate peak at 1460 cm^{-1} at 600 K.[27] The most convincing spectroscopic evidence for the assignment of the 1521 cm^{-1} IR peak to carbonate comes from the adsorption of CO on the Cs-modified Cu(110)−O surface at 360 K, which shows a strong peak at 1510 cm^{-1} assigned to ν(CO) of carbonate.[61] The corresponding C 1s and O 1s XP spectra show peaks at 289 and 531.2 eV, respectively, which are in good agreement with the spectra in Figures 3 and 4.[61] In addition, the strong 1500/1510 cm^{-1} peak was also observed from annealing adsorbed CO_2 as well as coadsorbed CO and O_2 on the Cs-modified Cu(110) surface.[61] Therefore, we identify the C_xO_y surface species formed after reduction of K/Cu_2O/Cu(111) by CO as carbonate (CO_3^{2-}). Since according to XPS, K has a +1 oxidation state (Figure 4, middle spectrum), it is likely that a K^+-CO_3^{2-} complex is formed, although it is not possible to determine the stoichiometry and surface bonding scheme from the current data. The three components of the carbonate peak likely arise from different bonding environments. Upon annealing, the appearance of the sharper and more symmetrical 1557 cm^{-1} peak is likely caused by the formation of more ordered structures of K^+-CO_3^{2-}.

In order to know the surface structural change during the reducing conditions, in situ STM images were taken under 3.5 × 10^{-4} Torr CO at room temperature (Figure 6). The as-prepared surface has a well-ordered Cu_2O-"44" row structure[62] across terraces. At a coverage less than 0.1 ML, potassium is well dispersed on the surface, either embedded or on the interface of the Cu_2O-"44" structure and Cu(111). Shortly after CO is introduced to the system, the reaction starts at defect sites, both at the Cu_2O and K sites (white circles in Figures 6A-C). The relaxation of the Cu_2O lattice appears near the step-edges as well as on the lower terrace after an ~40 min induction period (Figure 6C). This relaxation continues in Figure 6D, while the majority of Cu_2O row structure is maintained. Over time, the disorder of the Cu_2O-"44" structure expands, and metallic Cu forms near step-edges as well as in the middle of the terrace (Figure 6E). After this point, the reaction accelerates as evidenced by rapid formation and growth of metallic Cu regions (Figure 6F to Figure 6G). Ultimately, all Cu_2O is completely reduced, resulting in metallic Cu islands covering the surface (Figure 6H). Additionally, in Figure 6I, the Cu step edges are decorated by chains or small islands of a second species (imaged as dark) other than Cu. In accordance with the XP and IRRA spectra, this phase is assigned to the K^+-CO_3^{2-} complex formed after the reduction of K/Cu_2O/Cu(111). In our previous in situ study of Cu_2O/Cu(111) reduction by CO, no such second phase is observed, and the density of metallic Cu islands, mostly with circular shapes, is very low due to the mass transfer of released Cu atoms to step edges.[42] On the K-modified surface, while the smaller Cu islands are mobile and they have the tendency to merge into larger Cu islands (Figures 6H−I), the presence of the K^+-CO_3^{2-} chains slows down the free mass transfer of copper.

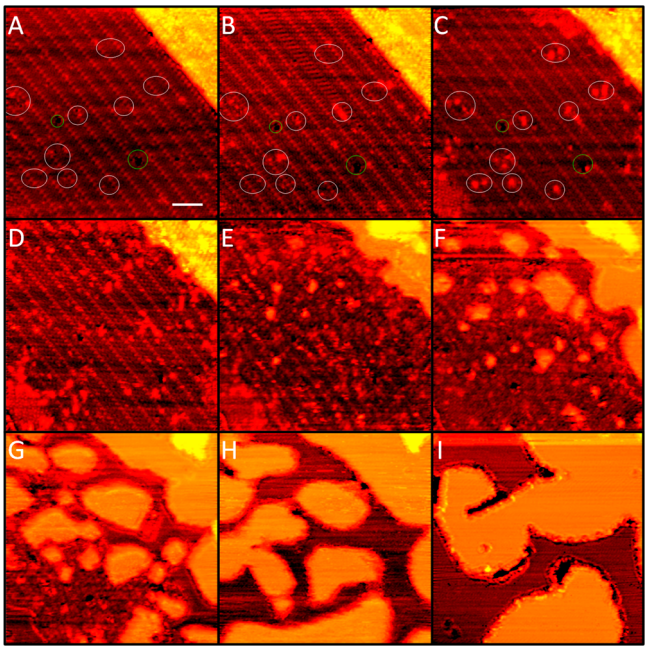

Figure 6. In situ STM images of 3.5 × 10^{-4} Torr CO reducing reoxidized potassium deposited Cu_2O/Cu(111) surface at room temperature. The exposure time from A) to H) is 0, 14.9, 42.3, 49.8, 52.2, 54.7, 57.2, and 62.2 min, respectively. I) is the image taken 6.7 min after CO was evacuated. Scanning conditions: 0.63 nA, 1.1 V (A to H); −0.63 nA, −1.06 V (I); scanning from bottom to top. White circles indicate defect sites, and green circles are landmarks. A) to H) are of the same area. The shared scale bar is 5 nm. Color corresponds to apparent height.

By changing scanning conditions, this C_xO_y species can be imaged as depressions (Figure 7A) or protrusions (Figure 7B). A zoomed-in image clearly resolves the near-square structural

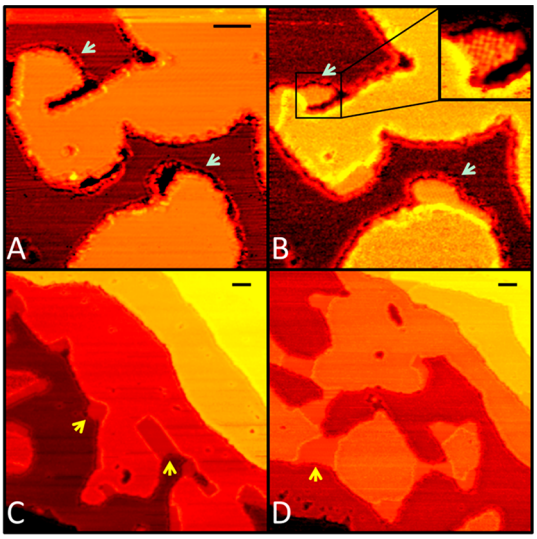

Figure 7. Postreaction topography of the reduced surface prepared in Figure 6. The CO evacuation time is A) 6.7 min; B) 55.3 min; C) 75.8 min; and D) 98.2 min. A) and B) are of the same area. The inset in B) is 6 × 6 nm^2. White arrows in A) and B) show the process of self-assembly of carbonates. Yellow arrows in C) and D) point to the location of carbonate islands. Scale bars are 5 nm. Scanning conditions: −0.63 nA, −1.06 V (A); −0.75 nA, −1.06 V (B to D); scanning from bottom to top. Color corresponds to apparent height.

pattern of this species (the inset in Figure 7B). The spacing of the periodic bright protrusions is ~0.41 nm. The number is very close to the smallest K−K distance of solid potassium overlayer on Cu(111).[63,64] Thus, we propose that the K^+-CO_3^{2-} complexes diffuse easily on the Cu(111) surface and self-assemble to form islands. As time progresses after CO evacuation, partial edges of Cu islands retract, and the neighboring carbonate phases expand (white arrows in Figures 7A and 7B). The self-assembled K^+-CO_3^{2-} islands occupy kink sites, the gaps between metallic Cu areas (yellow arrows in Figures 7C and 7D). These islands are highly mobile. The appearance of these islands can be linked to the 1557 cm^{-1} peak shown by IRRAS in Figure 5(b), and they are associated with the formation of well-ordered K^+-CO_3^{2-} islands. We estimate the K^+-CO_3^{2-} islands cover less than 10% of the surface, consistent with the initial coverage of K.

Despite the good spectroscopic agreement, the question remains whether the observation of chains and islands in STM is consistent with the presence of carbonates aggregation of carbonates or polycarbonate. Although evidence in the literature for the aggregation or chain formation of carbonates on surfaces is not abundant, it is not unprecedented. An STM study of carbonate formed by the reaction between CO_2 and O on Ag(110) shows that rod structures consisting of single or double chains of carbonates form between Ag−O rows and accumulate on step-edges.[65] In addition, carbonate produced from the adsorption of CO_2 on Cs/Cu(110) also shows chain-like structures by STM.[66] The polymerization of carbonate on the surface should also be considered since DFT calculations show that polycarbonates on ceria nanoparticles are stable although they have not been identified experimentally.[60] However, we cannot determine from the current experimental data whether polycarbonate chains are formed.

■ DISCUSSION

To understand how K promotes the reduction of Cu_2O/Cu(111) by CO, we first need to examine the effect of K on both the electronic structure of the surface and the adsorption of CO on the surface. A theoretical study of coadsorbed K and O on Rh(111) found that there is charge transfer from K to the antibonding states of O, resulting in the weakening of the O−Rh bond.[67] This was supported by experimental results from the HREELS study of Na+O/Ni(111)[68,69] and LEED of Cs +O/Ru(0001),[70] which suggest a weaker metal substrate−oxygen bond due to the presence of the alkali metals. Our previous DFT calculations show no charge transfer to the antibonding states is observed for both the O_L and O_U atoms, indicating that the K-promoted reduction of Cu_2O cannot be explained by the weakening of the Cu−O bond.[47]

Alkali metals are known to stabilize CO on various single crystal metal surfaces by strengthening the metal−CO bond and weakening the internal C−O bond. Little is known about how alkali metals affect CO adsorption on metal oxide films. In the case of Cu_2O/Cu(111), CO desorbs at ~180 K from both the bare and K-modified surfaces under UHV conditions. Theoretical calculations also show that the binding energy of CO on the K-modified "44" structure is −0.49 eV,[47] which is very close to a binding energy of −0.47 eV for CO adsorption on the bare "44" structure.[51] This shows that K neither promotes nor hinders the adsorption of CO on Cu_2O/Cu(111). However, while CO_2 does not adsorb on the "44" structure (BE = 0 eV), CO_2 adsorption is slightly more favorable on the K-modified surface with a binding energy of −0.47 eV. Carbonate is shown to be the most stable species on the K-modified "44" structure with a binding energy of −1.41 eV. This is in agreement with results reported in the literature on the coadsorption of CO_2 and alkali metals on various single crystal metal surfaces.[9]

According to our previous DFT calculations, the most active oxygen on the pure Cu_2O film during CO titration is the chemisorbed oxygen (O_{chem}) at the center of the 6-member ring,[51] which is occupied by K in the K/Cu_2O film and therefore not accessible. Among the lattice oxygens in the Cu_2O film (see Figure 1), the removal of the high-coordinated oxygens in the lower layer of the film (O_L) is found to be more favorable than those on the upper layer (O_U). Therefore, O_L seems likely to be involved in the formation of carbonate. Figure 8 shows the Gibbs reaction energy for the CO+O reaction on the bare and K-modified "44" structures. The blue and red curves represent the desorption of CO_2 as the product for the bare and K-modified surfaces, respectively, while the green curve represents the formation of surface carbonate as the product on the K-modified surface. It is clear that while there is no significant difference in reaction energy for CO_2 formation on either surface, the formation of surface carbonates on the K-modified surface is the most thermodynamically favorable process.

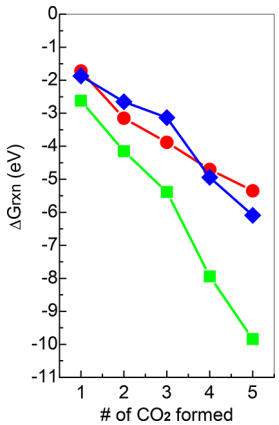

Figure 8. Gibbs reaction energy for CO titration under relatively high CO pressure at 298 K. Red: CO_2 formation on the 44 structure; Blue: CO_2 formation on 0.19 ML K deposited 44 structure; Green: CO_3^{2-} formation on 0.19 ML K deposited 44 structure.

■ SUMMARY AND CONCLUSIONS

In situ XPS data show that potassium promotes the reduction of Cu_2O/Cu(111) by CO as evidenced by the lower activation energy compared to the reduction of the bare surface. Both XPS and IRRAS data show the formation of CO_3^{2-} with O 1s and C 1s binding energies of 531.2 and 288.9 eV, respectively, and an OCO stretching mode at 1521 cm^{-1}. CO_3^{2-} is stable up to 500 K, and it likely forms a complex with the K^+ ions on the surface. STM images show that these K^+-CO_3^{2-} complexes form chains and small islands on the perimeters of reduced Cu islands, therefore hindering Cu mass transfer that was previously observed for the bare Cu_2O/Cu(111) surface. Following CO evacuation, STM images show the presence of ordered K^+-CO_3^{2-} islands. The formation of these ordered islands is likely a kinetic process that is also observed by IRRAS through heating the sample to ~400 K, in which a relatively sharp peak at 1557 cm^{-1} is observed. These results show the

role of K as a promoter and how it enhances the reduction of $Cu_2O/Cu(111)$ and provides a molecular level mechanism for the process. Theoretical calculations show that while K affects neither CO adsorption nor Cu−O bond stability, it stabilizes the formation of CO_3^{2-} on the surface. Since the formation of one CO_3^{2-} ion requires one CO molecule to react with two O atoms from the surface, the effect of the presence of K can then be described as the accelerated reduction of the Cu_2O film through the stabilization of CO_3^{2-} on the surface.

■ AUTHOR INFORMATION

Corresponding Author

*E-mail: djs@bnl.gov.

ORCID

Iradwikanari Waluyo: 0000-0002-4046-9722

Fang Xu: 0000-0002-8166-0275

Wei An: 0000-0002-0760-1357

Ping Liu: 0000-0001-8363-070X

J. Anibal Boscoboinik: 0000-0002-5090-7079

José A. Rodriguez: 0000-0002-5680-4214

Dario J. Stacchiola: 0000-0001-5494-3205

Present Addresses

[§]National Synchrotron Light Source II, Brookhaven National Laboratory, Upton, NY 11973.

[∥]SABIC-CRD at KAUST, Thuwal, Saudi Arabia.

[⊥]Department of Chemistry and Chemical Biology, Harvard University, Cambridge, MA 02138.

[#]College of Chemistry and Chemical Engineering, Shanghai University of Engineering Science, Shanghai 201620, P.R. China.

Notes

The authors declare no competing financial interest.

■ ACKNOWLEDGMENTS

This work was carried out at the Chemistry Department (STM, IRRAS, DFT) and used resources of the Center for Functional Nanomaterials (Computation, AP-XPS) and National Synchrotron Light Source (AP-XPS at beamline X1A1), Brookhaven National Laboratory, under Contract Nos. DE-SC0012704 and DE-AC02-98CH10886 with the U.S. Department of Energy, Office of Science, and supported by its Division of Chemical Sciences, Geosciences, and Biosciences within the Office of Basic Energy Sciences.

■ REFERENCES

(1) Aika, K.; Shimazaki, K.; Hattori, Y.; Ohya, A.; Ohshima, S.; Shirota, K.; Ozaki, A. Support and Promoter Effect of Ruthenium Catalyst. 1. Characterization of Alkali-Promoted Ruthenium Alumina Catalysts for Ammonia-Synthesis. *J. Catal.* **1985**, *92*, 296−304.

(2) Li, D.; Ichikuni, N.; Shimazu, S.; Uematsu, T. Catalytic Properties of Sprayed Ru/Al_2O_3 and Promoter Effects of Alkali Metals in CO_2 Hydrogenation. *Appl. Catal., A* **1998**, *172*, 351−358.

(3) Arai, M.; Nishiyama, S.; Tsuruya, S.; Masai, M. Effect of Alkali-Metal Promoter on Silica-Supported Copper Catalysts in Benzyl Alcohol Oxidation. *J. Chem. Soc., Faraday Trans.* **1996**, *92*, 2631−2636.

(4) Grant, R. B.; Lambert, R. M. Alkali-Metal Promoters and Catalysis - a Single-Crystal Investigation of Ethylene Epoxidation on Cs-Doped Ag(111). *Langmuir* **1985**, *1*, 29−33.

(5) Pedrero, C.; Waku, T.; Iglesia, E. Oxidation of CO in H_2-CO Mixtures Catalyzed by Platinum: Alkali Effects on Rates and Selectivity. *J. Catal.* **2005**, *233*, 242−255.

(6) Tanaka, H.; Ito, S. I.; Kameoka, S.; Tomishige, K.; Kunimori, K. Promoting Effect of Potassium in Selective Oxidation of CO in Hydrogen-Rich Stream on Rh Catalysts. *Catal. Commun.* **2003**, *4*, 1−4.

(7) Tanaka, H.; Kuriyama, M.; Ishida, Y.; Ito, S. I.; Tomishige, K.; Kunimori, K. Preferential CO Oxidation in Hydrogen-Rich Stream over Pt Catalysts Modified with Alkali Metals - Part I. Catalytic Performance. *Appl. Catal., A* **2008**, *343*, 117−124.

(8) Diehl, R. D.; McGrath, R. Structural Studies of Alkali Metal Adsorption and Coadsorption on Metal Surfaces. *Surf. Sci. Rep.* **1996**, *23*, 43−171.

(9) Politano, A.; Chiarello, G.; Benedek, G.; Chulkov, E. V.; Echenique, P. M. Vibrational Spectroscopy and Theory of Alkali Metal Adsorption and Co-Adsorption on Single-Crystal Surfaces. *Surf. Sci. Rep.* **2013**, *68*, 305−389.

(10) Netzer, F. P.; Doering, D. L.; Madey, T. E. Evidence for Molecular Reorientations on a Surface - Coadsorption of CO and Na on Ru(001). *Surf. Sci.* **1984**, *143*, L363−L370.

(11) Uram, K. J.; Ng, L.; Folman, M.; Yates, J. T. Direct Vibrational Spectroscopic Observations of Mixed Long-Range and Short-Range Adsorbate Interactions - the K + CO Interaction on Ni(111). *J. Chem. Phys.* **1986**, *84*, 2891−2895.

(12) Kondoh, H.; Orita, H.; Nozoye, H. Coadsorption of Cs and CO on Ru(001) - Formation of Cs+CO Islands and Isotope-Exchange of the CO Located inside the Islands. *J. Phys. Chem.* **1995**, *99*, 8790−8798.

(13) Seip, U.; Bassignana, I. C.; Kuppers, J.; Ertl, G. A TDS and HREELS Study of CO Adsorbed on a Potassium Promoted Fe(111) Surface. *Surf. Sci.* **1985**, *160*, 400−418.

(14) Gorling, A.; Ackermann, L.; Lauber, J.; Knappe, P.; Rosch, N. On the Coadsorption of CO and Alkali Atoms at Transition-Metal Surfaces - a Lcgto-Ldf Cluster Study. *Surf. Sci.* **1993**, *286*, 26−45.

(15) Alsarraf, N.; Stuckless, J. T.; King, D. A. Direct Measurement of Potassium-Promoted Change in Heat of Adsorption of CO on Ni(100). *Nature* **1992**, *360*, 243−245.

(16) Bonzel, H. P. Alkali-Metal-Affected Adsorption of Molecules on Metal-Surfaces. *Surf. Sci. Rep.* **1988**, *8*, 43−125.

(17) Wimmer, E.; Fu, C. L.; Freeman, A. J. Catalytic Promotion and Poisoning - All-Electron Local-Density-Functional Theory of CO on Ni(001) Surfaces Coadsorbed with K or S. *Phys. Rev. Lett.* **1985**, *55*, 2618−2621.

(18) Heskett, D.; Strathy, I.; Plummer, E. W.; Depaola, R. A. Photoemission and Electron-Energy-Loss Spectroscopy Investigation of CO+K/Cu(100). *Phys. Rev. B: Condens. Matter Mater. Phys.* **1985**, *32*, 6222−6237.

(19) Baba, M. F.; Mijoule, C.; Godbout, N.; Salahub, D. R. Coadsorption of K and CO on Pd Clusters - a Density-Functional Study. *Surf. Sci.* **1994**, *316*, 349−358.

(20) Lang, N. D.; Holloway, S.; Norskov, J. K. Electrostatic Adsorbate Adsorbate Interactions - the Poisoning and Promotion of the Molecular Adsorption Reaction. *Surf. Sci.* **1985**, *150*, 24−38.

(21) Rahman, T. S.; Stolbov, S.; Mehmood, F. Alkali-Induced Effects on Metal Substrates and Coadsorbed Molecules. *Appl. Phys. A: Mater. Sci. Process.* **2007**, *87*, 367−374.

(22) Stolbov, S.; Rahman, T. S. Alkali-Induced Enhancement of Surface Electronic Polarizibility. *Phys. Rev. Lett.* **2006**, *96*, 186801.

(23) Hoffmann, F. M.; Weisel, M. D.; Paul, J. The Activation of CO_2 by Potassium-Promoted Ru(001) 0.1. Ft-Iras and Tdms Study of Oxalate and Carbonate Intermediates. *Surf. Sci.* **1994**, *316*, 277−293.

(24) Paul, J.; Williams, G. P.; Hoffmann, F. M. Carbon Dioxide Activation and Alkali Compound Formation. I. Vibrational Characterization of Oxalate Intermediates. *Surf. Sci.* **2003**, *531*, 244−264.

(25) Wohlrab, S.; Ehrlich, D.; Wambach, J.; Kuhlenbeck, H.; Freund, H. J. Promoter Action of Alkali in the Activation of CO_2 on Pd(111) - a Hreels Case-Study. *Surf. Sci.* **1989**, *220*, 243−252.

(26) Liu, Z. M.; Zhou, Y.; Solymosi, F.; White, J. M. Vibrational Study of CO_2- on K-Promoted Pt(111). *J. Phys. Chem.* **1989**, *93*, 4383−4385.

(27) Hoffmann, F. M.; Yang, Y. X.; Paul, J.; White, M. G.; Hrbek, J. Hydrogenation of Carbon Dioxide by Water: Alkali-Promoted Synthesis of Formate. *J. Phys. Chem. Lett.* **2010**, *1*, 2130−2134.

(28) Mross, W. D. Alkali Doping in Heterogeneous Catalysis. *Catal. Rev.: Sci. Eng.* **1983**, *25*, 591−637.

(29) Koel, B. E.; Kim, J. Promoters and Poisons. In *Handbook of Heterogeneous Catalysis*; 2008; DOI: 10.1002/9783527610044.hetcat0087.

(30) Engvall, K.; Holmlid, L.; Kotarba, A.; Pettersson, J. B. C.; Menon, P. G.; Skaugset, P. Potassium Promoter in Industrial Ammonia Synthesis Catalyst: Studies by Surface Ionization. *Appl. Catal., A* **1996**, *134*, 239−246.

(31) Yang, Y.; Xiang, H.-W.; Xu, Y.-Y.; Bai, L.; Li, Y.-W. Effect of Potassium Promoter on Precipitated Iron-Manganese Catalyst for Fischer−Tropsch Synthesis. *Appl. Catal., A* **2004**, *266*, 181−194.

(32) Bowker, M. Chapter 7 - Promotion in Ammonia Synthesis. In *The Chemical Physics of Solid Surfaces*; King, D. A., Woodruff, D. P., Eds.; Elsevier: 1993; Vol. *6*, pp 225−268 DOI: 10.1016/B978-0-444-81468-5.50012-1.

(33) Stacchiola, D. J. Tuning the Properties of Copper-Based Catalysts Based on Molecular in Situ Studies of Model Systems. *Acc. Chem. Res.* **2015**, *48*, 2151−2158.

(34) Szanyi, J.; Goodman, D. W. CO Oxidation on a Cu(100) Catalyst. *Catal. Lett.* **1993**, *21*, 165−174.

(35) Domagala, M. E.; Campbell, C. T. The Mechanism of CO Oxidation over Cu(110) - Effect of CO Gas Energy. *Catal. Lett.* **1991**, *9*, 65−70.

(36) Klier, K. Methanol Synthesis. In *Advances in Catalyst*; Eley, D. D., Pines, H., Weisz, P. B., Eds.; Academic Press: 1982; Vol. *31*, p 243, DOI: 10.1016/S0360-0564(08)60455-1.

(37) Graciani, J.; Mudiyanselage, K.; Xu, F.; Baber, A. E.; Evans, J.; Senanayake, S. D.; Stacchiola, D. J.; Liu, P.; Hrbek, J.; Sanz, J. F.; et al. Highly Active Copper-Ceria and Copper-Ceria-Titania Catalysts for Methanol Synthesis from CO_2. *Science* **2014**, *345*, 546−550.

(38) Newsome, D. S. The Water-Gas Shift Reaction. *Catal. Rev.: Sci. Eng.* **1980**, *21*, 275−318.

(39) Jernigan, G. G.; Somorjai, G. A. Carbon-Monoxide Oxidation over 3 Different Oxidation-States of Copper - Metallic Copper, Copper (I) Oxide, and Copper (II) Oxide - a Surface Science and Kinetic-Study. *J. Catal.* **1994**, *147*, 567−577.

(40) Xu, F.; Mudiyanselage, K.; Baber, A. E.; Soldemo, M.; Weissenrieder, J.; White, M. G.; Stacchiola, D. J. Redox-Mediated Reconstruction of Copper During Carbon Monoxide Oxidation. *J. Phys. Chem. C* **2014**, *118*, 15902−15909.

(41) Yang, F.; Choi, Y. M.; Liu, P.; Hrbek, J.; Rodriguez, J. A. Autocatalytic Reduction of a Cu_2O/Cu(111) Surface by CO: STM, XPS, and DFT Studies. *J. Phys. Chem. C* **2010**, *114*, 17042−17050.

(42) Baber, A. E.; Xu, F.; Dvorak, F.; Mudiyanselage, K.; Soldemo, M.; Weissenrieder, J.; Senanayake, S. D.; Sadowski, J. T.; Rodriguez, J. A.; Matolin, V.; et al. In Situ Imaging of Cu_2O under Reducing Conditions: Formation of Metallic Fronts by Mass Transfer. *J. Am. Chem. Soc.* **2013**, *135*, 16781−16784.

(43) Hrbek, J.; Hoffmann, F. M.; Park, J. B.; Liu, P.; Stacchiola, D.; Hoo, Y. S.; Ma, S.; Nambu, A.; Rodriguez, J. A.; White, M. G. Adsorbate-Driven Morphological Changes of a Gold Surface at Low Temperatures. *J. Am. Chem. Soc.* **2008**, *130*, 17272−17273.

(44) Yang, F.; Choi, Y.; Liu, P.; Stacchiola, D.; Hrbek, J.; Rodriguez, J. A. Identification of 5−7 Defects in a Copper Oxide Surface. *J. Am. Chem. Soc.* **2011**, *133*, 11474−11477.

(45) Kresse, G.; Hafner, J. Abinitio Molecular-Dynamics for Liquid-Metals. *Phys. Rev. B: Condens. Matter Mater. Phys.* **1993**, *47*, 558−561.

(46) Kresse, G.; Furthmuller, J. Efficient Iterative Schemes for Ab Initio Total-Energy Calculations Using a Plane-Wave Basis Set. *Phys. Rev. B: Condens. Matter Mater. Phys.* **1996**, *54*, 11169−11186.

(47) Blochl, P. E. Projector Augmented-Wave Method. *Phys. Rev. B: Condens. Matter Mater. Phys.* **1994**, *50*, 17953−17979.

(48) Kresse, G.; Joubert, D. From Ultrasoft Pseudopotentials to the Projector Augmented-Wave Method. *Phys. Rev. B: Condens. Matter Mater. Phys.* **1999**, *59*, 1758−1775.

(49) Perdew, J. P.; Chevary, J. A.; Vosko, S. H.; Jackson, K. A.; Pederson, M. R.; Singh, D. J.; Fiolhais, C. Atoms, Molecules, Solids, and Surfaces - Applications of the Generalized Gradient Approximation for Exchange and Correlation. *Phys. Rev. B: Condens. Matter Mater. Phys.* **1992**, *46*, 6671−6687.

(50) Perdew, J. P.; Chevary, J. A.; Vosko, S. H.; Jackson, K. A.; Pederson, M. R.; Singh, D. J.; Fiolhais, C. Atoms, Molecules, Solids, and Surfaces - Applications of the Generalized Gradient Approximation for Exchange and Correlation (Vol 46, Pg 6671, 1992). *Phys. Rev. B: Condens. Matter Mater. Phys.* **1993**, *48*, 4978−4978.

(51) An, W.; Baber, A. E.; Xu, F.; Soldemo, M.; Weissenrieder, J.; Stacchiola, D.; Liu, P. Mechanistic Study of CO Titration on Cu_xO/Cu(111) ($X \leq 2$) Surfaces. *ChemCatChem* **2014**, *6*, 2364−2372.

(52) An, W.; Xu, F.; Stacchiola, D.; Liu, P. Potassium-Induced Effect on the Structure and Chemical Activity of the Cu_xO/Cu(111) ($X \leq 2$) Surface: A Combined Scanning Tunneling Microscopy and Density Functional Theory Study. *ChemCatChem* **2015**, *7*, 3865−3872.

(53) Monkhorst, H. J.; Pack, J. D. Special Points for Brillouin-Zone Integrations. *Phys. Rev. B* **1976**, *13*, 5188−5192.

(54) Robert, T.; Bartel, M.; Offergel, G. Characterization of Oxygen Species Adsorbed on Copper and Nickel Oxides by X-Ray Photoelectron Spectroscopy. *Surf. Sci.* **1972**, *33*, 123−130.

(55) Xu, F.; Mudiyanselage, K.; Baber, A. E.; Soldemo, M.; Weissenrieder, J.; White, M. G.; Stacchiola, D. J. Redox-Mediated Reconstruction of Copper During Carbon Monoxide Oxidation. *J. Phys. Chem. C* **2014**, *118*, 15902−15909.

(56) Sawyer, R.; Nesbitt, H. W.; Secco, R. A. High Resolution X-Ray Photoelectron Spectroscopy (Xps) Study of K2o-Sio2 Glasses: Evidence for Three Types of O and at Least Two Types of Si. *J. Non-Cryst. Solids* **2012**, *358*, 290−302.

(57) Wilde, M.; Beauport, I.; Stuhl, F.; Al-Shamery, K.; Freund, H. J. Adsorption of Potassium on Cr_2O_3(0001) at Ionic and Metallic Coverages and Uv-Laser-Induced Desorption. *Phys. Rev. B: Condens. Matter Mater. Phys.* **1999**, *59*, 13401−13412.

(58) Joseph, Y.; Ketteler, G.; Kuhrs, C.; Ranke, W.; Weiss, W.; Schlogl, R. On the Preparation and Composition of Potassium Promoted Iron Oxide Model Catalyst Films. *Phys. Chem. Chem. Phys.* **2001**, *3*, 4141−4153.

(59) Faraggi, M. N.; Rogero, C.; Arnau, A.; Trelka, M.; Ecija, D.; Isvoranu, C.; Schnadt, J.; Marti-Gastaldo, C.; Coronado, E.; Gallego, J. M.; et al. Role of Deprotonation and Cu Adatom Migration in Determining the Reaction Pathways of Oxalic Acid Adsorption on Cu(111). *J. Phys. Chem. C* **2011**, *115*, 21177−21182.

(60) Vayssilov, G. N.; Mihaylov, M.; St Petkov, P.; Hadjiivanov, K. I.; Neyman, K. M. Reassignment of the Vibrational Spectra of Carbonates, Formates, and Related Surface Species on Ceria: A Combined Density Functional and Infrared Spectroscopy Investigation. *J. Phys. Chem. C* **2011**, *115*, 23435−23454.

(61) Carley, A. F.; Roberts, M. W.; Strutt, A. J. Activation of Carbon-Monoxide and Carbon-Dioxide at Cesium-Promoted Cu(110) and Cu(110)-O Surfaces. *J. Phys. Chem.* **1994**, *98*, 9175−9181.

(62) Jensen, F.; Besenbacher, F.; Laegsgaard, E.; Stensgaard, I. Oxidation of Cu(111) - 2 New Oxygen Induced Reconstructions. *Surf. Sci.* **1991**, *259*, L774−L780.

(63) Fan, W. C.; Ignatiev, A. Growth of an Orientationally Ordered Incommensurate Potassium Overlayer and Its Order-Disorder Transition on the Cu(111) Surface. *Phys. Rev. B: Condens. Matter Mater. Phys.* **1988**, *37*, 5274−5277.

(64) Watanabe, K.; Inoue, K.; Nakai, I. F.; Fuyuki, M.; Matsumoto, Y. Ultrafast Electron and Lattice Dynamics at Potassium-Covered Cu(111) Surfaces. *Phys. Rev. B: Condens. Matter Mater. Phys.* **2009**, *80*, 075404.

(65) Guo, X. C.; Madix, R. J. Carbonate on Ag(110): A Complex System Clarified by Stm. *Surf. Sci.* **2001**, *489*, 37−44.

(66) Carley, A. F.; Davies, P. R.; Harikumar, K. R.; Jones, R. V.; Roberts, M. W. Reactivity and Structural Aspects of Cesium and

Oxygen States at Cu(110) Surfaces: An Xps and Stm Investigation. *J. Phys. Chem. B* **2004**, *108*, 14518−14526.

(67) Liu, Z. P.; Hu, P. An Insight into Alkali Promotion: A Density Functional Theory Study of CO Dissociation on K/Rh(111). *J. Am. Chem. Soc.* **2001**, *123*, 12596−12604.

(68) Politano, A.; Formoso, V.; Agostino, R. G.; Colavita, E.; Chiarello, G. Evidences of Alkali-Induced Softening of the Oxygen-Substrate Bond. *J. Chem. Phys.* **2008**, *128*, 074703.

(69) Politano, A.; Formoso, V.; Chiarello, G. Alkali Adsorption on Ni(111) and Their Coadsorption with CO and O. *Appl. Surf. Sci.* **2008**, *254*, 6854−6859.

(70) Over, H.; Bludau, H.; Skottkeklein, M.; Moritz, W.; Ertl, G. Low-Energy Electron-Diffraction Analysis of the Structure of a Cs-O/Ru(0001) Coadsorbate Phase. *Phys. Rev. B: Condens. Matter Mater. Phys.* **1992**, *46*, 4360−4363.

(71) Toomes, R. L.; King, D. A. Coadsorption and Surface Compound Formation in the Interaction of CO_2 with K on Co{1010}. *Surf. Sci.* **1996**, *349*, 65−80.

(72) Onsgaard, J.; Storm, J.; Christensen, S. V.; Nerlov, J.; Godowski, P. J.; Morgen, P.; Batchelor, D. The Interaction of CO_2 with Potassium-Promoted Cu(100) - Adsorption, Reactions and Radiation-Induced Dissociation of CO_2. *Surf. Sci.* **1995**, *336*, 101−112.

(73) Farkas, A. P.; Solymosi, F. Activation and Reactions of CO_2 on a K-Promoted Au(111) Surface. *J. Phys. Chem. C* **2009**, *113*, 19930−19936.

(74) Binet, C.; Badri, A.; Boutonnetkizling, M.; Lavalley, J. C. Ftir Study of Carbon-Monoxide Adsorption on Ceria - CO_2(2-) Carbonite Dianion Adsorbed Species. *J. Chem. Soc., Faraday Trans.* **1994**, *90*, 1023−1028.